Applied Catalysis B: Environmental 89 (2009) 651–658

Contents lists available at ScienceDirect

Applied Catalysis B: Environmental

journal homepage: www.elsevier.com/locate/apcatb

Fenton-driven regeneration of MTBE-spent granular activated carbon—Effects of particle size and iron amendment procedures

Scott G. Huling [a,*], Eunsung Kan [b,1], Caleb Wingo [c,2]

[a] U.S. Environmental Protection Agency, Office of Research and Development, National Risk Management Research Laboratory, Robert S. Kerr Environmental Research Center, P.O. Box 1198, Ada, OK 74820, United States
[b] Dept. of Chemical and Petroleum Engineering, United Arab Emirates University, Al-Ain, P.O. Box 17555, United Arab Emirates
[c] East Central University, College of Health and Sciences, 1100 E. 14th, Ada, OK 74820, United States

ARTICLE INFO

Article history:
Received 31 October 2008
Received in revised form 5 January 2009
Accepted 5 February 2009
Available online 12 February 2009

Keywords:
Activated carbon
Hydrogen peroxide
Iron
Methyl-*tert*-butyl ether
Oxidation

ABSTRACT

Fenton-driven regeneration of spent granular activated carbon (GAC) can be used to regenerate organic contaminant-spent GAC. In this study, the effects of GAC particle size (>2 mm to <0.35 mm) and acid pre-treatment of GAC on Fenton-driven oxidation of methyl-*tert*-butyl ether (MTBE)-spent GAC were evaluated. Iron (Fe) was amended to the GAC using two methods: (1) untreated—where GAC was amended with a concentrated solution of ferrous sulfate and (2) acid pre-treatment—where GAC was amended with acid followed by sequential applications of a dilute ferrous sulfate solution. Subsequently, MTBE was amended to the GAC, followed by oxidative treatments with H_2O_2. H_2O_2 reaction and MTBE oxidation were inversely correlated with GAC particle size and were attributed to shorter intraparticle diffusion transport distances for both H_2O_2 and MTBE. Image analysis of the GAC cross-sections (i.e., prepared thin sections) revealed that the Fe amended to the GAC extended to the center of the GAC particles. Fe accumulated at higher levels on the periphery of the untreated GAC but Fe dispersal was more uniform in the acid pre-treated GAC. In the acid pre-treated GAC, conditions for MTBE oxidation were favorable and greater levels of MTBE oxidation were measured for all particle size fractions tested. Modeling and critical analysis of H_2O_2 diffusive transport and reaction indicated limited H_2O_2 penetration into large GAC particles which contributed to a decline in MTBE removal. Residual MTBE remaining on the GAC limited the quantity of MTBE that could be re-adsorbed, but no reduction in MTBE sorption capacity resulted from oxidative treatments.

Published by Elsevier B.V.

1. Introduction

There may be as many as 250,000 releases of methyl-*tert*-butyl ether (MTBE) associated with leaking underground fuel tanks in the U.S. [1]. Consequently, millions may be at increased risk of exposure to MTBE from ground water contamination since a large number of the United States population relies on ground water for drinking water [2]. Liquid phase adsorption of MTBE with granular activated carbon is a proven technology with high mechanical reliability and effective removal. Selection of activated carbon adsorption for treatment of MTBE-contaminated ground water, relative to other viable technologies, requires a detailed assessment of site-specific factors including water quality, process conditions (i.e., flow rate, influent concentration, the presence of other contaminants), and type of carbon [3]. Once the GAC is spent with MTBE, it is regenerated and placed back in service (i.e., reused), replaced with virgin GAC, or disposed. In the majority of cases involving GAC regeneration, the spent GAC is thermally regenerated either on-site or transported to a thermal regeneration facility and regenerated off-site. Fenton-driven, on-site regeneration of spent GAC is being developed to transform contaminants into less toxic byproducts, re-establish the sorptive capacity of the carbon for the target chemical(s), increase the useful life of the GAC, and reduce costs for GAC regeneration and water or air treatment.

Fenton-driven regeneration of MTBE-spent GAC involves the addition of hydrogen peroxide (H_2O_2) to iron (Fe)-amended GAC. In this reaction, H_2O_2 reacts with ferrous iron (Fe(II)) resulting in the production of hydroxyl radicals ($^{\bullet}OH$) (Reaction (1)). $^{\bullet}OH$ are non-selective and rapidly react with a wide array of organic contaminants, including MTBE (1.6×10^9 L/mol s) [4,5]. Continuous formation of $^{\bullet}OH$ occurs in the Fenton mechanism via side reactions in which ferrous Fe is regenerated from ferric Fe (Reactions (1)–(3)) [6]:

$$Fe(II) + H_2O_2 \rightarrow Fe(III) + {}^{\bullet}OH + OH^- \quad (1)$$

* Corresponding author. Tel.: +1 580 436 8610; fax: +1 580 436 8614.
E-mail addresses: huling.scott@epa.gov (S.G. Huling), ekan@uaeu.ac.ae (E. Kan), caljwin@email.ecok.edu (C. Wingo).
[1] Tel.: +971 50 112 1287.
[2] Tel.: +1 580 436 8654; fax: +1 580 436 8614.

0926-3373/$ – see front matter. Published by Elsevier B.V.
doi:10.1016/j.apcatb.2009.02.002

Table 1
GAC particle size, fraction of total mass in 8 × 30, and Fe concentration.

Sieve range	GAC particle diameter (mm)	Average GAC particle size (mm)	Fraction of GAC mass in 8 × 30[a] (%)	Fe concentration (added) (mg/kg)[b]	
				Untreated	Acid pre-treated
>10	>2	>2	14.4	5960	5110
10 × 16	1.18–2	1.59[c]	68.6	5960	4830
16 × 30	0.6–1.18	0.89[c]	14.2	5930	5240
30 × 45	0.36–0.6	0.48[c]	1.7	5970	4410
<45	<0.36	<0.36	0.49	5960	5200
8 × 30	0.6–2.36	1.54[a]	–	–	5060

[a] Weighted average generated from GAC fractions contained in 8 × 30.
[b] Fe added to the GAC: untreated average = 5960 mg/kg, 95% confidence interval (CI) 5940–5970 mg/kg (n = 5); acid pre-treated average = 5090 mg/kg, 95% CI = 4890–5290 mg/kg (n = 4) (excluding 30 × 45); background Fe is 1030 mg/kg (Huling et al. [10]).
[c] Average particle size = average of largest and smallest particle sizes in the size range.

$$Fe(III) + H_2O_2 \rightarrow Fe(II) + {}^{\bullet}O_2^{-} + 2H^{+} \quad (2)$$

$$Fe(III) + {}^{\bullet}O_2^{-} \rightarrow Fe(II) + O_2 \quad (3)$$

Intraparticle MTBE mass transfer and mass transport from the GAC solid to the bulk fluid involves the following steps: (1) desorption from solid to liquid phase, (2) diffusive transport within the pores involving pore and surface diffusion, (3) diffusive transport through a quiescent film surrounding the particle, and (4) advective transport into the bulk solution [7,8]. The rate-limiting mechanism may be simplified to pore diffusion limitation if contaminant desorption is fast relative to pore diffusion [9]. In Fenton-driven regeneration of GAC, MTBE oxidation in the aqueous phase results in steep concentration gradients adjacent to GAC surfaces causing enhanced MTBE desorption and intraparticle diffusive transport outward from the GAC particle. Simultaneously, H_2O_2 undergoes reactive–diffusive transport from the bulk solution into the GAC particle where it reacts predominantly with immobilized Fe in the GAC [10]. Overall, the rate and extent of MTBE oxidation in GAC is potentially limited by the penetration depth of Fe-amended to, and immobilized in the GAC, the rate of H_2O_2 diffusive transport into the GAC and the rate of MTBE diffusion from the GAC.

The pH at point of zero charge (pH_{PZC}) of GAC is the pH where the net surface charge of solid surfaces is neutral (i.e., positive charges = negative charges) [11]. Acidic treatment of GAC oxidizes the carbon surfaces through the addition of acidic surface oxide functional groups [12] resulting in a reduction of the pH_{PZC} [13]. When the solution pH > pH_{PZC}, the carbon surface is covered by deprotonated carboxyl groups (i.e., acidic surface oxide functional groups); the negative charges attract and adsorb cations from solution, serve as anchoring sites for Fe, and favor higher dispersion of metal catalysts [14]. However, the exact mechanism for improved Fe dispersal in the GAC is not well defined. Often, Fe amendment to GAC has been accomplished using strongly acidic Fe solutions [15–18] where the pH of the Fe solution is less than the pH_{PZC} of the GAC. It is proposed to use experimental conditions consistent with Tseng and Wey [14] where the pH of the Fe solution amended to the GAC is greater than the pH_{PZC} of the GAC.

Conceptually, MTBE oxidation occurs in a "reaction zone" established in the GAC particle where Fe, MTBE and H_2O_2 temporarily co-exist [19]. In small GAC particles, it is proposed that the diffusive transport distances required for H_2O_2 and MTBE are shorter, diffusive transport limitations are fewer, and the potential for MTBE oxidation is greater. Additionally, Fe amendment procedures (described in Section 2.2, below) that result in greater Fe penetration and dispersal in the GAC will result in a larger reaction zone where Fe, MTBE, and H_2O_2 co-exist and result in conditions favorable for MTBE oxidation.

The objectives of this study were to investigate the effects of GAC particle size and Fe amendment procedures (i.e., acid pre-treatment of GAC) on Fenton regeneration of MTBE-spent GAC, and the limiting mechanisms of intraparticle diffusive transport.

2. Methods and materials

2.1. GAC sieving and particle size

The GAC (8 × 30 mesh, Calgon Carbon Corp., Pittsburg, PA) was derived from bituminous coal. The GAC was sieved using a series of sieves with mesh sizes of 10, 16, 30, and 45 producing different particle size ranges (>10, 10 × 16, 16 × 30, 30 × 45, <45) (Table 1). The GAC was liberally rinsed with de-ionized (DI) water, dried in an oven at 105 °C (24 h) and stored in a dessicator until used.

2.2. Fe amendment

The optimal Fe concentration in GAC was determined to be ~6710 mg/kg (1020 mg/kg background; 5690 mg/kg amended) [10] and therefore used as a guideline in this study. GAC (9 g) from each sieve range fraction was placed into glass reactors (250 mL Erlenmeyer flasks) and saturated with DI water (>24 h). Two methods of Fe amendment were used. A ferrous sulfate solution (27 mL, 1.93 g/L as Fe^{2+}) was amended to the untreated GAC and placed on a shaker table (100 rpm, 1 h). After 3 days contact time, the solution was decanted and measured for Fe.

The second method involved acidic pre-treatment of GAC (9 g). Nitric acid (HNO_3 1.5 mL) was amended to the GAC slurry to reduce the pH (pH 3.0–3.4) and pH_{PZC} of the GAC prior to Fe amendment. Subsequently, a dilute solution of ferrous sulfate (pH 5.3; 0.25 L; 70 mg/L as soluble Fe^{2+}) was added to each reactor and allowed >3 days contact time. The Fe amendment procedure was repeated twice more. The large volume of dilute Fe solution was required to prevent Fe precipitation and to amend an equal mass of Fe to the GAC as in the untreated GAC Fe amendment procedure. The final Fe solution was decanted and measured for Fe. In both methods, DI water (10 mL) was added and decanted (3×) to remove sulfate. DI water (20 mL) was added to each reactor, allowed 7 days contact time and measured for pH.

2.3. pH point of zero charge (pH_{PZC})

The pH_{PZC} of the GAC was determined using the pH drift method [11]. De-ionized (DI) water (50 mL) amended with NaCl (0.01 M) was placed in 100 mL amber vials and sparged with N_2 (10–15 min; >200 mL/min) to eliminate CO_2 and to stabilize pH. The pH was adjusted (pH 2–11) in a series of vials by adding either HCl or NaOH while purging the headspace with N_2. GAC (0.15 g) was added to the vial and was capped immediately. The final pH

(pH_{FINAL}) was measured in each of the vials after 48 h and plotted versus the initial pH ($pH_{INITIAL}$). The pH_{PZC} was determined graphically at the intersection of pH_{FINAL} and the line, $pH_{FINAL} = -pH_{INITIAL}$. The pH and pH_{PZC} of GAC received from Calgon Carbon (Pittsburg, PA) was 5.0 and 5.1, respectively (refer to Supporting Information, Fig. SI-1).

Below is a summary of measured pH values for various experimental conditions in GAC slurries and Fe solutions.

Experimental condition	pH	pH pH_{PZC}	Comment
GAC slurry (background)	5.0–5.1		"as received" GAC
pH_{PZC} (background)		5.1	
Acid-treated GAC slurry (final)	3.0–3.4		Treated with nitric acid to
pH_{PZC}		4.2–4.5	lower the pH_{PZC}
Fe solution concentrated	2.6		27 mL, 1.93 g/L Fe^{2+} (1×);
Fe solution dilute	5.3		0.25 L, 70 mg/L Fe^{2+} (3×)
Pre-oxidation	3.4–3.5		pH in acid pre-treated
Post-oxidation	3.0–3.1		and untreated GAC slurries

2.4. MTBE amendment

The MTBE adsorption step was performed by amending an MTBE solution (0.12 L, 2.91–3.0 mg/L) to water-saturated, Fe-amended GAC (9 g GAC; pH 3.4–3.5) in 250 mL Erlenmeyer flasks wrapped in aluminum foil and parafilmed. The MTBE solution was allowed 4 days contact time for adsorption. Post-sorption aqueous samples (replicates) were collected and analyzed for MTBE and used to determine the initial mass of MTBE on GAC.

2.5. Oxidation

H_2O_2 (3.4 mL, 30%) was added to each reactor ($[H_2O_2]_{INITIAL} \sim 19.5$ g/L) and mixed (100 rpm) until the H_2O_2 was depleted. After 24 h, the procedure was repeated for a total of six applications. In a previous study, low variation in the H_2O_2 reaction rate was measured between H_2O_2 applications. Therefore, the H_2O_2 concentration was measured in each reactor during the third oxidation event to quantify the H_2O_2 degradation rate constant.

2.6. Post-oxidation

Replicate aqueous and GAC samples were collected for MTBE analysis. Post-oxidation GAC samples (1.5 g, 3 g, 6 g, and 9 g wet weight) were re-amended with MTBE (48 mL, 1.18 mg/L). Subsequently, post-sorption aqueous and GAC MTBE concentrations were plotted to develop Freundlich isotherms. These isotherms were used to determine the $[MTBE]_{GAC}$ corresponding with the initial MTBE aqueous concentration in equilibrium with the virgin GAC, which was then used to estimate percent regeneration. Although there are several methods used to measure percent regeneration of GAC, this method provides the most accurate measure since MTBE loading should be measured at the same equilibrium liquid phase MTBE concentration in both the virgin and regenerated GAC [20].

2.7. Analytical

A detailed description of the analytical procedures used in this study is provided in the Supporting Information (Section I. Analytical methods and materials) and have been provided in previous studies [10,17,18]. These methods and materials were used to analyze MTBE in the aqueous phase and in the GAC, H_2O_2, iron, and pH.

Post-sorption and post-oxidation concentrations of MTBE in water were measured by purge and trap gas chromatography (GC). MTBE in GAC (~1 g GAC) was extracted with 10 mL methanol and analyzed by GC, mass spectrometry. H_2O_2 was measured using a titanium sulfate reagent [21]. Total Fe was measured in the aqueous solution using the phenanthroline method [22]. The absorbance of the H_2O_2–$TiSO_4$ complex and the chelated Fe was measured at 407 nm and 510 nm, respectively using a Jenway 6505 UV/VIS Spectrophotometer. An Orion Sure-Flow ROSS Combination pH meter was used to monitor the pH.

2.8. Image analysis of GAC polished thin sections

Imaging and microanalysis of GAC particles were conducted using scanning electron microscopy (SEM) with energy dispersive X-ray spectrometry (EDS). Thin sections of GAC particles were examined with a JEOL scanning electron microscope (Model JSM-6360, Montgomery, TX) with a beam current of 10 nA. The microscope is equipped with an Oxford Instruments energy dispersive X-ray spectrometer (Model 6587) with high resolution germanium detectors. GAC thin sections were coated with gold for SEM and EDS analysis. For surface elemental composition analyses, the acceleration voltage was 20 keV and the surface area interrogated by EDS (47,000 μm^2/site) represented approximately 0.3–4.2% of the external surface area of 8 × 30 GAC particles (i.e., assuming spherical GAC particles).

Polished thin sections of GAC samples were vacuum embedded in 3 M Scotchcast #3 Electrical Resin and mounted on high purity fused quartz glass slides with superglue (Spectrum Petrographics, Vancouver, WA). Imaging and microanalysis of polished GAC thin sections was conducted using SEM/EDS to assess the depth-dependent elemental composition of GAC particles. Image areas (7.5 μm × 10 μm) on randomly selected GAC particles ($n = 3$) were located at various distances between the edge and the center of the GAC particle.

3. Results and discussion

3.1. Acid treatment and Fe amendment

Acidic treatment of the GAC reduced the pH from 5.0 to 3.0–3.4. The pH_{PZC} of the acid pre-treated GAC ($pH_{PZC} = 4.2$–4.5; pH 3.0–3.4) was reduced from background ($pH_{PZC} = 5.1$) and was lower than the pH of the Fe solution amended to the GAC (pH 5.3) (refer to Supporting Information, Fig. SI-1). Under this condition, negative charges on the GAC surface attract and adsorb cations in solution (i.e., Fe^{2+} and Fe^{3+}) and favor greater dispersion of the metal catalysts in the GAC [14].

GAC particle size did not have a significant effect on the accumulation of Fe in the untreated or acid pre-treated GAC (Table 1). Relatively high residual $[Fe^{2+}]_{AQUEOUS}$ was measured in the acid pre-treated GAC (30 × 45) reactor resulting in lower $[Fe]_{GAC}$. There is no firm explanation why this occurred. The residual Fe and volume of solution in the acid-treated GAC suspension ($[Fe]_{AQUEOUS} = 10.0$ mg/L ($n = 18$); 0.25 L (three applications)) were greater than in the untreated GAC (8.3 mg/L ($n = 5$); 27 mL). Consequently, Fe retention was greater in the untreated GAC (average 99.9%) than in the acid pre-treated GAC (average 84.6%) where approximately 15% less Fe was amended (5090 mg/kg) than in the untreated GAC (5960 mg/kg) (Table 1). Although oxidative modification of the GAC surfaces through acidic pre-treatment yielded more Fe sorption sites, other factors (discussed below) played a role in Fe dispersal and immobilization in GAC.

3.2. Image analysis of GAC polished thin sections

SEM/EDS analysis and elemental quantification of polished thin sections of GAC were used to assess the Fe dispersal in (16 × 30) GAC particles. The radial distance measured from the center of the GAC particle towards the outside edge, was normalized to the radius to account for different size particles within the same sieve range. For example, the radial distance/radius = 0, 0.33, 0.67, and 1 represent the center, 1/3, 2/3 and outside edge, respectively. Relative to Fe-unamended GAC, Fe levels were significantly greater in the Fe-amended GAC (i.e., untreated and acid pre-treated) and extended from the outside edge to the center of the GAC particle (Fig. 1). Greater accumulation of Fe was measured on the periphery of the untreated, Fe-amended GAC relative to the acid-treated GAC. This result is consistent with a previous investigation using a SEM/EDS method to assess Fe distribution in GAC where the interrogation depth was limited to ~20 μm [10]. In the current study, SEM/EDS analysis involved the entire cross-sectional depth of the GAC particles. These results indicate uniform dispersal and complete penetration of Fe throughout the acid pre-treated GAC.

The exact mechanism for improved Fe dispersal in the acid pre-treated GAC is not well defined and may be attributed to multiple mechanisms. In the acid pre-treated GAC slurry (pH 3.0–3.4), sorption sites are predominantly occupied by protons (H^+). During Fe amendment, displacement of H^+ by Fe ions (Fe^{2+} and Fe^{3+}) in the dilute solution was not instantaneous and required several days (>3 days) to approach equilibrium. In the untreated, Fe-amended GAC slurry (pH 5.0), sorption sites on the GAC surface were sparsely occupied by H^+, allowing rapid (i.e., 1–2 h) exchange of H^+ by Fe^{2+} and possibly other Fe sorption mechanisms. The high ionic strength of the concentrated Fe solution (27 mL; 1.93 g/L; pH 2.6; untreated GAC) allows closer proximity between Fe ions in solution and GAC surfaces resulting in greater probability of contact, sorption, and immobilization. For example, the large volume of dilute Fe solution (0.25 L, 70 mg/L, pH 5.3, three applications) amended to the acid pre-treated GAC had significantly lower ionic strength and dispersive forces resulting in a decline in the rate and extent of Fe adsorption. Using selective chemical extraction procedures, it was previously determined that freshly amended Fe in GAC was predominantly comprised of poorly ordered, amorphous Fe and organically bound Fe [10]. Background Fe(III) or freshly amended amorphous Fe(III), in conjunction with the high stability of Fe(III)–O–Fe(II) interactions (i.e., immobilized Fe(III) and amended Fe^{2+}), represents a probable mechanism [23] by which the amended Fe^{2+} is immobilized in the GAC. Consequently, other reactions (i.e., precipitation and complexation) and immobilization mechanisms could be compounded in the Fe-rich periphery of the GAC.

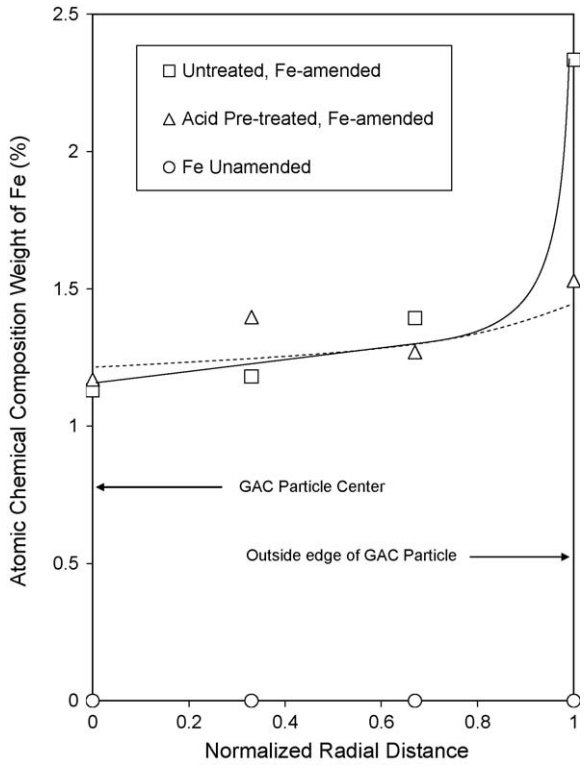

Fig. 1. Atomic chemical composition of iron in GAC particle cross-section. Results are from SEM/EDS image analysis ($n = 3$) of GAC (16 × 30) polished thin sections. Sample locations (i.e., distances) from the edge of the GAC particle were normalized to the radius of the GAC particle. The normalized radial distances (distance/radius) of 0, 0.33, 0.67, and 1 represent the center, 1/3, 2/3 and outside edge, respectively. Distances were normalized to account for different size particles within the same sieve range. The average particle size analyzed was 660 μm.

3.3. H_2O_2 degradation

H_2O_2 reaction kinetics were pseudo-first order and inversely proportional to GAC particle size (Fig. 2; refer also to Supporting Information, Figs. SI-2 and SI-3). Despite the differences in Fe amendment procedures and lower Fe concentration in the acid pre-treated GAC (Table 1), pseudo-first order reaction rate constants were nearly the same (Fig. 2). The 8 × 30 GAC was comprised predominately (69%) of particles in the (10 × 16) sieve size range (Table 1) and consequently, H_2O_2 reaction was most similar between the (8 × 30) and (10 × 16) GAC (Fig. 2). Due to the accumulation of Fe on the periphery of the untreated GAC (Fig. 1), even limited H_2O_2 penetration would result in significant contact and reaction between the Fe and H_2O_2. In the acid pre-treated GAC, Fe dispersal was more uniform and deeper H_2O_2 penetration would be required to achieve comparable contact between H_2O_2 and Fe.

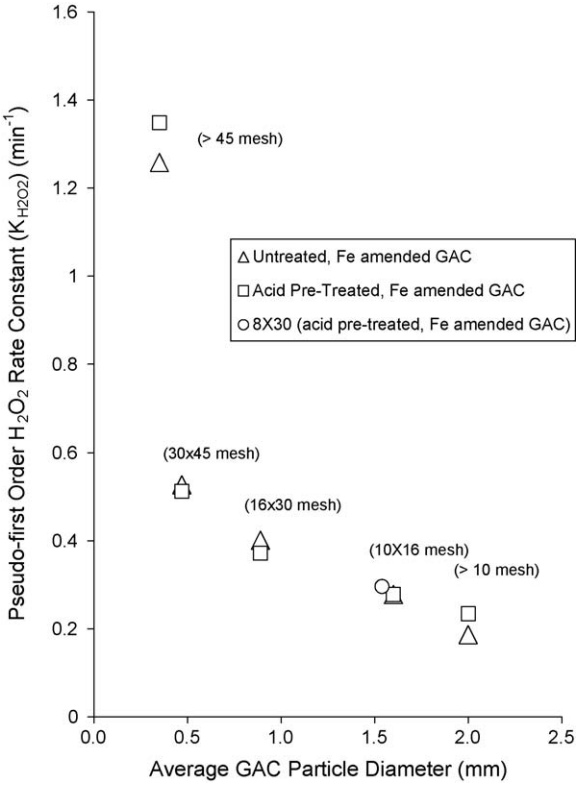

Fig. 2. Pseudo-first order H_2O_2 reaction rate constants ($k_{H_2O_2}$) as a function of GAC particle size (untreated and acid pre-treated, Fe-amended GAC).

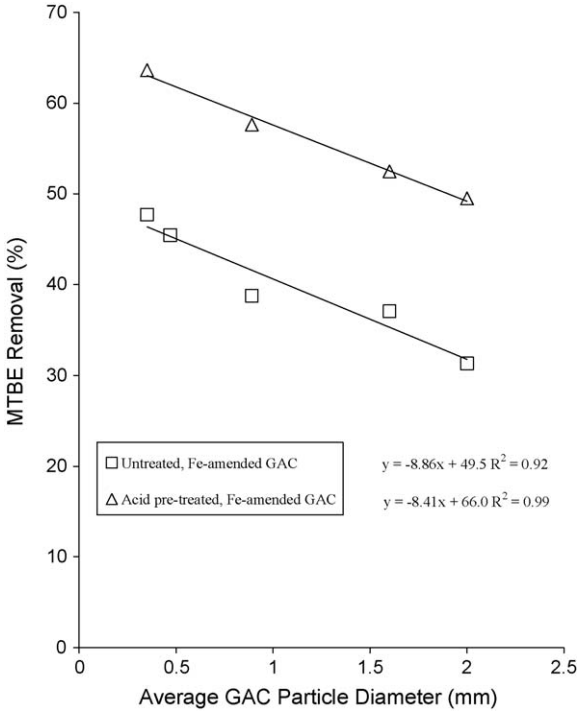

Fig. 3. MTBE removal percentages as a function of GAC particle size (untreated and acid pre-treated, Fe-amended GAC fractions).

3.4. MTBE oxidation

The average initial MTBE concentration in GAC was 39.2 mg/kg and 37.2 mg/kg in the acid pre-treated and untreated GAC, respectively. MTBE removal in the GAC via oxidative treatments was greater (15–20%) for each size fraction of the acid pre-treated GAC than in the untreated GAC (Fig. 3). The pH in acid-treated and untreated reactors was approximately the same before oxidation (pH 3.4–3.5) and after oxidation (pH 3.0–3.1). Acid treatment and more uniform Fe dispersal into the GAC particle resulted in greater MTBE oxidation (Fig. 3). When Fe, H_2O_2, and MTBE co-exist, conditions for Fenton-driven oxidation of MTBE are favorable. A linear and predictable trend between MTBE removal and the size of GAC particles alludes to the role of shorter transport distances in small GAC particles and lower intraparticle diffusive transport limitations for MTBE and H_2O_2. Differences in GAC particle size do not result in differences in the properties of the GAC. For example, GAC comprised of three different raw materials (bituminous, lignite, and wood), ground into different particle size fractions, was found to have similar physical and chemical properties as the bulk GAC [24]. Therefore, the observed trends in MTBE oxidation and removal are attributed to the transport limitations inherent with GAC particle size.

3.5. GAC regeneration

GAC regeneration efficiency (Eq. (I)) was estimated based on the following parameters: MTBE concentration resulting from the MTBE re-adsorbed to regenerated GAC (S_R) (Eq. (II)); and the pre-oxidation MTBE concentration on the virgin GAC (S_V) (Eq. (III)) [20]. This method of estimating regeneration efficiency is based on the quantity of adsorbate re-amended to regenerated GAC relative to virgin GAC and does not include the post-oxidation residual quantity of adsorbate on the carbon. The most conservative method of determining regeneration efficiency is by measuring S_R and S_V using the same equilibrium aqueous phase concentrations (i.e., $[MTBE]_F$) thus assuring a uniform basis of comparison [20]. Post-oxidation Freundlich isotherms were prepared using GAC from each particle size fraction (refer to Supporting Information, Section IV, post-oxidation sorption isotherms, Fig. SI-4):

$$\text{Regeneration efficiency}\ (\%) = \frac{S_R}{S_V} \times 100 \quad \text{(I)}$$

$$S_R = \frac{([MTBE]_I - [MTBE]_F) \times V}{M_{GAC,\,REGENERATED}\ (mg/g)} \quad \text{(II)}$$

$$S_V = \frac{([MTBE]_I - [MTBE]_F) \times V}{M_{GAC,\,VIRGIN}\ (mg/g)} \quad \text{(III)}$$

where $[MTBE]_I$ and $[MTBE]_F$ = initial and final MTBE aqueous concentrations, respectively (mg/L), V = volume of adsorbate solution applied (L) and M_{GAC} = mass of GAC (g).

Post-oxidation Freundlich isotherms were used to estimate the MTBE concentration on regenerated GAC in equilibrium with the aqueous phase MTBE concentration that corresponded with the MTBE aqueous phase concentration initially in equilibrium with the virgin GAC. GAC regeneration results were variable (42–72%) and a clear trend was not established with particle size (Table 2). As defined, regeneration efficiency could be adversely affected by either the treatment-dependent loss of MTBE adsorption capacity attributed to carbon deterioration, or by incomplete carbon regeneration. Here, the ratio of cumulative MTBE mass to initial MTBE mass was slightly greater than 100% in all cases (Table 2) suggesting that GAC deterioration and a reduction in sorption capacity did not result from oxidative treatments. Rather, residual MTBE remaining on the GAC limited the sorption sites and the quantity of MTBE that could be re-adsorbed. Results are consistent with another study where no loss in MTBE sorption capacity resulted from rigorous Fenton-driven regeneration of GAC [18].

3.6. Intraparticle H_2O_2 diffusive transport

Intraparticle H_2O_2 diffusive transport and reaction provides insight to the relative size of the reaction zone and the extent of MTBE removal measured in GAC particles of different size. H_2O_2 diffusion in macroporous solids is functionally dependent on the

Table 2
Regeneration measurements of MTBE-spent, acid pre-treated GAC and ratio of the final and initial $[MTBE]_{GAC}$.

Reactor	Initial $[MTBE]_{GAC}$ [a] (mg/kg)	Regeneration (%)	Final $[MTBE]_{GAC}$ [b] (mg/kg)	Final/initial $[MTBE]_{GAC}$ [c] (%)
8 × 30	39.3	49	40.3	102.5
>10	39.2	51	40.7	103.9
10 × 16	39.2	42	41.5	105.9
16 × 30	39.1	46	40.4	103.2
<45	39.1	72	44.2	113.1

[a] Initial MTBE concentration on virgin GAC.
[b] 2nd post-sorption $[MTBE]_{GAC}$ = post-oxidation residual MTBE + MTBE re-adsorbed to regenerated GAC.
[c] Ratio of final $[MTBE]_{GAC}$ (regenerated GAC) and the initial $[MTBE]_{GAC}$ × 100. The final $[MTBE]_{GAC}$ = post-oxidation $[MTBE]_{GAC}$ + MTBE re-adsorbed to the regenerated GAC.

tortuosity in the GAC (Eq. (IV)). Tortuosity (τ_f) is the ratio of the actual transport distance to the shortest (direct) pathway distance. A tortuosity factor of 1 indicates that the actual transport pathway is equal to the shortest transport pathway and tortuosity is negligible. A τ_f value of 10 for H_2O_2 in activated carbon [25] was assumed to represent the tortuosity conditions in this study due to similarities in raw materials and physical characteristics:

$$D_{H_2O_2,GAC} = \frac{D_{H_2O_2,w}}{\tau_f} \quad \text{(IV)}$$

where $D_{H_2O_2,GAC}$ = diffusivity of H_2O_2 in water saturated GAC (cm^2/s), $D_{H_2O_2,w}$ = diffusivity of H_2O_2 in water (Table 1) (cm^2/s) and τ_f = tortuosity (dimensionless).

H_2O_2 diffusion and reaction in GAC was examined using a two-dimensional (radial), time-dependent mathematical equation (Eq. (V)). This equation was used to quantify H_2O_2 concentrations as a function of time and transport distance in GAC. A numerical differential equation solver (Berkeley Madonna, version 8.3, Berkeley Madonna Inc., CA, USA) was used to solve Eq. (V):

$$\frac{\partial C}{\partial t} = D_{H_2O_2,GAC}\left(\frac{2}{r}\frac{\partial C}{\partial r} + \frac{\partial^2 C}{\partial r^2}\right) - k_{H_2O_2}C \quad \text{(V)}$$

where,

C = concentration of H_2O_2 (mg/L)
r = radius of GAC particle (μm) and
$k_{H_2O_2}$ = pseudo-first order H_2O_2 reaction rate constant (s^{-1}).

H_2O_2 reaction rates in the acid-treated, Fe-amended reactors were simulated using Eq. (V) in GAC particles of different size (0.36 mm ≤ GAC diameter ≤ 2 mm; 25 °C). GAC particles were assumed to have a spherical shape and uniform Fe distribution (i.e., acid-treated, Fe-amended). H_2O_2 reaction was modeled using pseudo-first order kinetics, consistent with experimental results (Fig. 2; also, refer also to Supporting information, Figs. SI-2 and SI-3). Simulations involved segmented GAC particles with 10 differential volumes (spherical shells) and equal radii ($r_e = r/10$) from the GAC center (i.e., r_e = 0.036 mm and 0.2 mm for GAC radius r = 0.36 mm and 2 mm, respectively). The thickness of an outer layer extending beyond the carbon particle was sized in a manner to assure the H_2O_2 concentration was similar to the bulk phase concentrations measured in the study. Therefore, the H_2O_2 concentration on the outside edge of the first layer of the carbon particle corresponded with measured H_2O_2 concentrations in the reactor. Simulations for three separate differential volumes (spherical shells) of the GAC particle were critically analyzed (i.e., the outer-most, midpoint, and inner-most differential volumes).

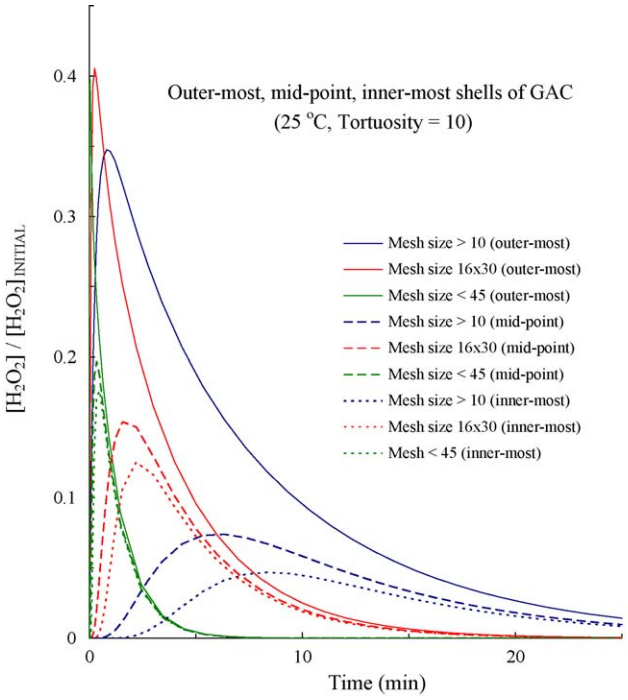

Fig. 4. H_2O_2 penetration into GAC particles during oxidation (25 °C, $[H_2O_2]_{INITIAL}$ ~22 g/L, tortuosity factor, τ_f = 10). Simulations are presented for the outer-most, midpoint, and inner-most differential volumes of an idealized spherical GAC particle. The average diameter of the GAC particles is >2 mm (mesh >10), 0.89 mm (mesh 16 × 30), and <0.36 mm (mesh size <45).

Model results suggest that higher H_2O_2 concentrations penetrate deeper into small GAC particles relative to large GAC particles, but persists for shorter periods due to higher H_2O_2 reaction rates (Fig. 4). Conditions for MTBE oxidation are favorable in the reaction zone when H_2O_2, MTBE, and Fe co-exist, i.e., refer to the volume of the reaction zone (V_{RZ}) in Fig. 5. Exterior of the GAC particle, MTBE

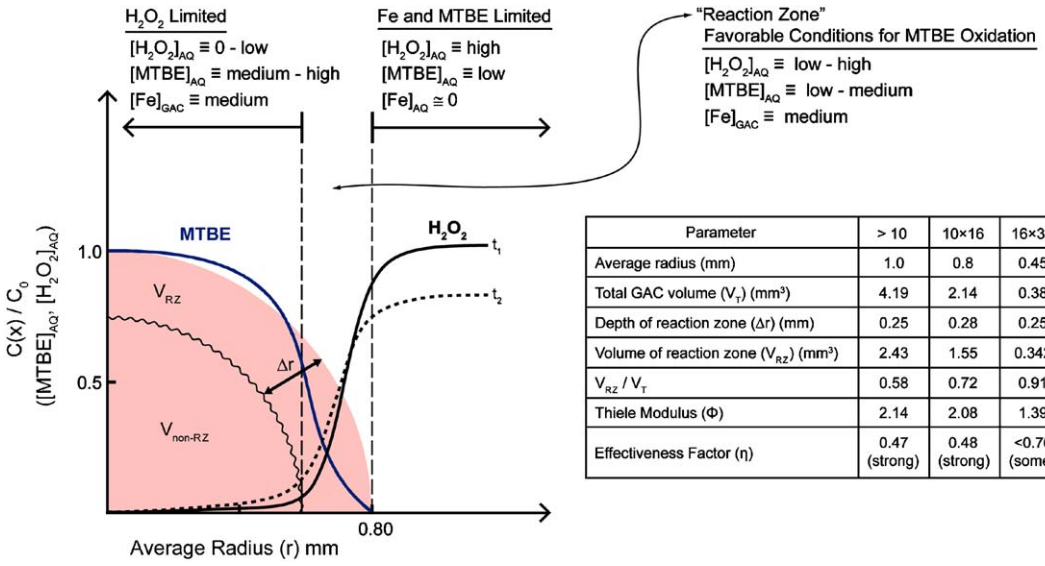

Parameter	> 10	10×16	16×30	< 45
Average radius (mm)	1.0	0.8	0.45	0.18
Total GAC volume (V_T) (mm^3)	4.19	2.14	0.38	0.0244
Depth of reaction zone (Δr) (mm)	0.25	0.28	0.25	> 0.18
Volume of reaction zone (V_{RZ}) (mm^3)	2.43	1.55	0.342	0.0244
V_{RZ} / V_T	0.58	0.72	0.91	1.00
Thiele Modulus (Φ)	2.14	2.08	1.39	0.97
Effectiveness Factor (η)	0.47 (strong)	0.48 (strong)	<0.76 (some)	0.76 (some)

Fig. 5. Conceptual model of H_2O_2 penetration into GAC particles. The H_2O_2 penetration depth was used to estimate the width and volume of the reaction zone.

oxidation in solution is limited due to low concentrations of MTBE and Fe. In the interior of the GAC particle and the reaction zone (i.e., the volume of the non-reaction zone, $V_{non\text{-}RZ}$, refer to Fig. 5), low concentrations of H_2O_2 limit the Fenton reaction and, consequently, conditions for MTBE oxidation are unfavorable.

3.7. Volume of reactive zone within GAC particles

The H_2O_2 diffusion–reaction transport modeling results were used to estimate the relative volume of the reaction zone based on the estimated penetration depth of H_2O_2. Time-dependent H_2O_2 concentrations were estimated for ten differential volumes (spherical shells) in the GAC particle with equal radii ($r_e = r/10$) from the GAC center. The reaction zone (Δr) (Fig. 5; refer to inset table) was selected to be the distance in which 15% of the initial H_2O_2 concentration fully penetrated the GAC particle (refer to Supporting Information, Figs. SI-5a–SI-5e). Assuming spherical geometry of the GAC particle and estimated values for the depth of the reaction zone (Δr), the volume of the reaction zone (V_{RZ}) and the total volume (V_T) of the GAC particle were computed (see inset table in Fig. 5). Based on this analysis, the ratio of the volume of reaction zone and total volume (V_{RZ}/V_T) is inversely correlated with GAC particle size. Therefore, H_2O_2 penetrates a larger fraction of the GAC in progressively smaller particles, contacts a larger total mass of the GAC in the reactor, and MTBE oxidation is more favorable.

3.8. Dimensionless Thiele modulus

The dimensionless Thiele-modulus (Φ) is a diagnostic tool that can be used to critically analyze the relative roles of intraparticle diffusion and reaction in porous media [25,26] (refer to Supporting Information, Section 6, Thiele modulus (Φ) analysis and calculations). The effectiveness factor (η) is a measure of the reduction in the H_2O_2 reaction rate attributed to H_2O_2 diffusion limitations in pores and is the ratio of the actual and the ideal H_2O_2 reaction rates (assuming no diffusional limitation) [26]. For, $\Phi \ll 1$, $\eta = 1$, indicating no pore diffusion limitations and no reduction in reaction; $\Phi = 1$, $\eta \cong 0.76$ indicates some limitation, and $\Phi \gg 1$, $\eta \cong 1/\Phi$ indicates strong pore diffusion limitations [26]. Given measured values for $k_{H_2O_2}$ (Fig. 2) and tortuosity-corrected values of $D_{H_2O_2,EFF}$ (Eq. (II)), Thiele modulus (Φ) values were 2.14, 2.08, 1.39, and 0.97 for sieve sizes >10, 10 × 16, 16 × 30, and <45, respectively (refer to Fig. 5, see inset Table; and Supporting Information, Section 6, Thiele modulus analysis and calculations). Thiele modulus results indicate that strong diffusion limitations would occur in large GAC particles (>10, 10 × 16) and some diffusion limitations would occur in smaller GAC particles (16 × 30, <45). Given that (8 × 30) GAC is comprised of 83% by weight of (>10, 10 × 16) (Table 1), strong H_2O_2 diffusion transport limitations are also projected in the bulk GAC (8 × 30).

Both the H_2O_2 diffusion–reaction modeling (Eq. (III)) and Thiele modulus calculations indicate H_2O_2 diffusion limitations in large GAC particles (>10, 10 × 16, 8 × 30). H_2O_2 reactive–diffusive transport modeling indicates full or nearly full penetration of H_2O_2 in <45 and 16 × 30 GAC particles, respectively, while Thiele modulus calculations indicate that some H_2O_2 diffusion limitations occurred. The criteria used in calculating the volume of the reaction zone using H_2O_2 modeling (i.e., penetration of $0.15 \times [H_2O_2]_{INITIAL}$), indicated full penetration in <45 GAC particles. However, H_2O_2 concentrations at these levels (i.e., 85% of the initial H_2O_2 was fully reacted) indicate some diffusion transport limitations. Therefore, results between these two methods of analysis are in agreement. Overall, intraparticle diffusive transport of H_2O_2 limits penetration and reaction in large GAC particles.

3.9. MTBE mass transfer, transport, and oxidation

H_2O_2 consumption is dominated by reaction with GAC-bound Fe and therefore the majority of H_2O_2 consumption occurs within the porous structure of the GAC and not with Fe in the bulk solution [10]. H_2O_2 reaction and formation of $^{\bullet}OH$ at the carbon surface is ideal due to the proximity of high soluble MTBE concentrations and the high probability of reaction between $^{\bullet}OH$ and MTBE.

Initially, when H_2O_2 is amended to the GAC slurry, $[MTBE]_{AQUEOUS}$ is maximum in both the interior and exterior of the GAC particle (Fig. 5) and oxidation efficiency is highest. As oxidation proceeds, $[MTBE]_{AQUEOUS}$ declines, $[MTBE]_{GAC}$ declines in the periphery of the GAC particle, and intraparticle MTBE diffusive transport begins to play a limiting role in MTBE oxidation, especially in larger GAC particles. Under this non-equilibrium sorption condition, reverse aqueous concentration gradients result due to the outward diffusive transport of MTBE, and the inward diffusive transport of H_2O_2. Small GAC particles, exhibiting shorter transport distances for both MTBE and H_2O_2, result in the steepest MTBE concentration gradients, and fastest MTBE desorption and diffusive transport. Consequently, higher concentrations of reactants occur in the reaction zone over a larger volume of the GAC particle resulting in greater MTBE transformation and removal.

4. Conclusions

Fe was amended to GAC in different particle size ranges (>2 mm to <0.35 mm) (i.e., sieve ranges <45, 30 × 45, 16 × 30, 10 × 16, and >10) using two methods: (1) acid pre-treatment followed by Fe amendment with a dilute ferrous sulfate solution (0.25 L; 70 mg/L as Fe^{2+}; pH 5.3; three applications) and (2) untreated GAC amended with a concentrated ferrous sulfate solution (27 mL; 1.93 g/L as Fe^{2+}; pH 2.6). GAC particle size did not have a significant effect on the accumulation of Fe in GAC using either Fe amendment method. Approximately 15% more Fe was immobilized in the untreated GAC (5960 mg/kg) than the acid pre-treated GAC (5100 mg/kg). In the acid pre-treated GAC, uniform dispersal of Fe extended to the center of the GAC particle. In the Fe-amended, untreated GAC, dispersal was less uniform and Fe accumulated on the periphery of the GAC and extended to the GAC center. H_2O_2 reaction was inversely proportional with GAC particle size indicating greater contact between Fe and H_2O_2. Despite differences in Fe amendment procedures (i.e., untreated, acid pre-treated), similar H_2O_2 reaction rates were measured in GAC particles of the same size (<45, 30 × 45, 16 × 30, 10 × 16, and >10). Fe-driven catalysis of H_2O_2 in GAC forms reactive species that transform methyl-*tert*-butyl ether. MTBE oxidation was greater for all size fractions in the acid pre-treated GAC where Fe dispersal was more uniform. Residual MTBE remaining on the GAC limited the quantity of MTBE that could be re-adsorbed, but no reduction in MTBE sorption capacity resulted from oxidative treatments. Modeling and critical analysis of H_2O_2 diffusive transport and reaction indicated limited H_2O_2 penetration into large GAC particles which contributed to a decline in MTBE removal. Greater H_2O_2 penetration and reaction, and greater MTBE removal in smaller GAC particles underscores the importance of particle size and diffusive transport limitations.

Conflict of interest

The U.S. Environmental Protection Agency, through its Office of Research and Development, funded and managed the research described here. It has not been subjected to Agency review and therefore does not necessarily reflect the views of the Agency, and no official endorsement should be inferred.

Acknowledgements

The authors acknowledge Dr. R.G. Arnold, Dr. W.P. Ela, and Dr. R.E. Sierka (University of Arizona) for their valuable input on transport and reaction mechanisms, and M. Blankenship, T. Pardue, and Dr. B. Pivetz (Shaw Environmental Inc., Ada, OK) for their assistance.

Appendix A. Supplementary data

Supplementary data associated with this article can be found, in the online version, at doi:10.1016/j.apcatb.2009.02.002.

References

[1] R. Johnson, J. Pankow, D. Bender, C. Price, J. Zogorski, Environ. Sci. Technol. 34 (2000) 210A–217A.
[2] M.J. Moran, J.S. Zogorski, P.J. Squillace, Ground Water 43 (2005) 615–627.
[3] J. Sutherland, C. Adams, J. Kekobad, Water Res. 38 (2004) 193–205.
[4] G.V. Buxton, C. Greenstock, W.P. Hellman, A.B. Ross, J. Phys. Chem. Ref. Data 17 (1988) 513–886.
[5] A.A. Burbano, D.D. Dionysiou, M.T. Suidan, Water Res. 42 (2008) 3225–3239.
[6] J.D. De Laat, G.T. Le, B. Legube, Chemosphere 55 (2004) 715–723.
[7] J. Crittenden, D.W. Hand, H. Arora, B.W. Lykins, AWWA 79 (1987) 74–82.
[8] C. De Las Casas, K. Bishop, L. Bercik, M. Johnson, M. Potzler, W. Ela, A.E. Saez, S.G. Huling, R.G. Arnold, in: C. Clark, A. Lindner, ACS Symposium Series 940 (Eds.), American Chemical Society, Washington D.C., 2006; pp. 43–65.
[9] J. Crittenden, N. Hutzler, D. Geyer, J. Oravitz, G. Friedman, Water Resour. Res. 22 (1986) 271–284.
[10] S.G. Huling, K.P. Jones, T. Lee, Environ. Sci. Technol. 41 (2007) 4090–4096.
[11] M.V. Lopez-Ramona, F. Stoecklib, C. Moreno-Castilla, F. Carrasco-Marina, Carbon 37 (1999) 1215–1221.
[12] T. Karanfil, J.E. Kilduff, Environ. Sci. Technol. 33 (1999) 3217–3224.
[13] H. Huang, M. Lu, J. Chen, C. Lee, Chemosphere 51 (2003) 935–941.
[14] H.H. Tseng, M.Y. Wey, Chemosphere 62 (2006) 756–766.
[15] L.C. Toledo, A.C.B. Silva, R. Augusti, R.M. Lago, Chemosphere 50 (2003) 1049–1054.
[16] D.S. Kim, J. Hazard. Mater. 106B (2004) 67–84.
[17] S.G. Huling, R.G. Arnold, R.A. Sierka, P.K. Jones, D.K. Fine, J. Environ. Eng. 126 (2000) 595–600.
[18] S.G. Huling, P.K. Jones, E.P. Wendell, R.G. Arnold, Water Res. 39 (2005) 2145–2153.
[19] E. Kan, S.G. Huling, Environ. Sci. Technol. 43 (5) (2009) 1493–1499.
[20] R.M. Narbaitz, J. Cen, Water Res. 31 (1997) 2532–2542.
[21] S.G. Huling, R.G. Arnold, R.A. Sierka, M.A. Miller, Environ. Sci. Technol. 32 (1998) 3436–3441.
[22] APHA, AWWA, WEF Standard Methods for the Examination of Water and Wastewater, Method 3500-Fe D, Phenanthroline Method, in: L.S. Clesceri, A.E. Greenberg, R.R. Trussell (Eds.), 17th ed., 1989, pp. 3-102–3-106.
[23] E.E. Roden, J.M. Zachara, Environ. Sci. Technol. 30 (1996) 1618–1628.
[24] A.G. Patni, D.K. Ludlow, C.D. Adams, J. Environ. Eng. 134 (2008) 216–221.
[25] A. Georgi, F. Kopinke, Appl. Catal. B-Environ. 58 (2005) 9–18.
[26] L.D. Schmidt, The Engineering of Chemical Reactions, Oxford University Press, New York, 1998, pp. 536.